Application of locality principle to radio occultation studies of the Earth's atmosphere and ionosphere

A. G. Pavelyev[1], Y.A. Liou[2], S.S. Matyugov[1], A.A. Pavelyev[1], V.N. Gubenko[1], K. Zhang[3], and Yu. Kuleshov[4]

[1]Kotelnikov Institute of Radio Engineering and Electronics of the Russian Academy of Sciences, Fryazino, Moscow region, Russia

[2]Center for Space and Remote Sensing Research, National Central University, Chung-Li,

320, Taiwan

[3]SPACE Research Centre/RMIT University/Australia (03) 99253272

kefei.zhang@rmit.edu.au

[4] National Climate Centre, Bureau of Meteorology, Melbourne, Australia

Received: 23 October 2014 – Accepted: 8 December 2014 – Published: 20 January 2015

Correspondence to: A.G. Pavelyev (alxndr38@mail.ru)

Published by Copernicus Publications on behalf of the European Geosciences Union.

Abstract

A new formulation of previously introduced principle of locality is presented. The principle can be applied for modernization of the radio occultation (RO) remote sensing of the atmospheres and ionospheres of the Earth and planets. The principle states that the main contributions to variations of the amplitude and phase of the radio waves passing through a layered medium are connected with influence of the vicinities of tangential points where the refractivity gradient is perpendicular to the radio ray trajectory. The RO method assumes spherical symmetry of the investigated medium. In this case if location of a tangent point relative to the spherical symmetry center is known, the derivatives on time of the RO signal phase and Doppler frequency variations can be recalculated into the refractive attenuation. Several important findings are consequences of the locality principle: (i) if position of the center of symmetry is known, the total absorption along the ray path can be determined at a single frequency; (ii) in the case of low absorption the height, displacement from the radio ray perigee, and tilt of the inclined ionospheric (atmospheric) layers can be evaluated; (iii) the contributions of the layered and irregular structures in the RO signal can be separated and parameters of layers and turbulence can be measured at a single frequency using joint analysis of the amplitude and phase variations. Specially for the Earth's troposphere, the altitude distributions of the weak total absorption (about of 1-4 db) of the radio waves at GPS frequencies corresponding to possible influence of the oxygen and water vapor can be measured with accuracy of about 0.1 db at a single frequency. According with the locality principle, a new index of ionospheric activity is introduced. This index is measured from the phase variations of radio waves passing through the ionosphere. Its high correlation with S4 scintillation index is established. This correlation indicates the significant influence of locally spherical symmetric ionospheric layers on variations of the phase and amplitude of the RO signal passing through transionospheric communication links. Obtained results expand the applicable domain of the RO method as a powerful remote sensing technique for geophysical and meteorological research.

1 Introduction

The radio occultation (RO) remote sensing has been known during the last 50 years as a powerful tool for investigation of the atmospheres, ionospheres and planetary surfaces (Fjeldbo, 1964, Marouf and Tyler, 1986, Lindal et al., 1983, 1987; Hinson et al., 1997, 1999; Yunck et al., 2000; Yakovlev, 2002, and references therein). With regard to the study of near-Earth space the RO method should be competitive with other means of remote sensing (Gurvich and Krasilnikova, 1987; Yunck et al., 1988; Melbourne et al., 1994; Yakovlev, 2002; Liou et al., 2010). Assumption of spherical symmetry – cornerstone of RO method – should be carefully analyzed when the RO technology is applied to global monitoring of the Earth' ionosphere and atmosphere at different altitudes (Vorob'ev and Krasilnikova, 1994; Melbourne et al., 1994, Syndergaard 1998, 1999; Yunck et al., 2000). In particular, effectiveness of the RO method applied for investigation of the Earth's ionosphere can be compared with radio tomographic approach (Kunitsyn and Tereshchenko, 2003). The tomographic method allows obtaining 2-D distributions of electron density in the ionosphere using chain of ground-based receivers, which capture signals of Low Earth Orbital (LEO) or navigational satellites along a set of intersecting radio rays (Kunitsyn et al., 2011, 2013). Unlike the radio tomographic approach, the RO method used a set of nearly parallel radio ray's trajectories. This enforces to use for processing the assumption of spherical symmetry of the Earth's ionosphere and atmosphere with known location of the center of symmetry (Melbourne et al, 1994; Yakovlev, 2002; Melbourne, 2004). According with this assumption all resulting altitude profiles of atmospheric and ionospheric parameters are attached to vertical and horizontal coordinates of the radio ray perigee relative to the spherical symmetry center, which is close to or coincident with the center of the Earth or planet.

Highly stable signals synchronized by atomic frequency standards and radiated by GPS satellites at frequencies F1=1575.42 MHz and F2=1227.60 MHz, create at the altitudes from 0 to 20 000 km radio fields that can be used for the development of the radio occultation (RO) method as a new tool for global monitoring of the ionosphere and neutral atmosphere (Gurvich and Krasilnikova, 1987; Yunck, 1988). During 1995 – 2014 the LEO missions: GPS/MET (Melbourne et al., 1994; Ware et al., 1996; Gorbunov et al. 1996; Kursinski et al., 1997; Vorob'ev et al., 1997), SAC-C (Schmidt et al., 2005), CHAMP (Wickert et al., 2001), FORMOSAT-3 (Liou et al., 2007; Fong et al., 2008), GRACE (Hajj et al., 2004; Wickert et al., 2005), METOP (Engeln et al., 2011; Joo et al., 2012), TERRA-SAR, TANDEM-X (Zus et al., 2014), and FY-3 CNOS (Bai et al., 2014) demonstrated that the RO technique is a powerful remote sensing tool for obtaining key vertical profiles of bending angle, refractivity, temperature, pressure and water vapour in the atmosphere and electron density in ionosphere with global coverage, high spatial and temporal resolution (Zhang et al., 2013). Important contributions have been introduced also in (i) the theory of radio wave propagation (Gorbunov and Gurvich, 1998a; Gorbunov et al., 2002; Benzon et al., 2003; Gorbunov and Lauritsen, 2004; Gorbunov and Kirchengast, 2005; Pavelyev et al., 2004, 2010a, b, 2011a, 2013a), (ii) climate changes detection (Kirchengast et al., 2000; Steiner et al., 2001; Foelsche et al., 2008), (iii) space weather effects and ionosphere monitoring (Rius et al., 1998; Jakowski et al., 2004; Wickert et al., 2004; Arras et al., 2008, 2010; Pavelyev et al., 2002, 2004, 2010a, b, 2011a, b; 2012), (iv) deriving new radio-holographic methods of the RO remote sensing (Karayel and Hinson, 1997; Mortensen and Hoeg, 1998; Pavelyev, 1998, 2013; Gorbunov and Gurvich, 1998b; Mortensen et al., 1999; Hocke et al., 1999; Gorbunov, 2002; Gorbunov et al., 1996, 2002, 2010; Igarashi et al., 2000; Jensen et al. 2003, 2004; Pavelyev et al., 2002, 2004, 2010a, b, 2012, 2013a, b; Liou et al., 2010).

Recently, an important connection between the intensity and derivatives on time of the phase, eikonal, Doppler frequency of radio waves propagating through the ionosphere and atmosphere has been discovered by theoretical analysis and confirmed by processing of the RO radio-holograms (Liou and Pavelyev, 2006; Liou et al., 2007, 2010; Pavelyev et al., 2008a, 2012, 2013). This connection is a key regularity of the RO method. Now this relationship gets a possibility to recognize that the phase (eikonal) acceleration (proportional to the time derivative of the Doppler shift) has the same importance for the theory of radio waves propagation in a layered medium and solution of the RO inverse problem as the Doppler frequency, phase path excess, and refractive attenuation of the RO signal (Liou and Pavelyev, 2006; Liou et al., 2007; Pavelyev 2008, 2013; Pavelyev et al., 2009, 2010a, b, 2012, 2013). It follows from this connection that the phase acceleration technique allows one to convert the phase and Doppler frequency changes into refractive attenuation variations at a single frequency. Note that this is similar to classical dynamic when the derivations of the path and velocity on time and acceleration are connected by the second Newton’s law. From such derived refractive attenuation and amplitude data, one can estimate the integral absorption of radio waves. This is important for future RO missions when measuring water vapor and minor atmospheric gas constituents, because the difficulty of removing the refractive attenuation effect from the amplitude data can be avoided. The phase acceleration technique can be applied also for determining the location and inclination of sharp layered plasma structures (including sporadic Es layers) in the ionosphere. The advantages of the phase acceleration technique are validated by analyzing RO data from the Challenging Minisatellite Payload (CHAMP) and the FORMOSA Satellite Constellation Observing Systems for Meteorology, Ionosphere, and Climate missions (FORMOSAT-3/COSMIC).

The locality principle generalizes the phase path excess acceleration/intensity technique to the practically important case in which the position of the center of symmetry of layered medium is unknown (Pavelyev et al., 2012, 2013; Pavelyev 2013). New relationships have been revealed that expanding the scope and applicable domain of the RO method. These relationships allow, in particular, measuring the real height, inclination, and displacement of atmospheric and ionospheric layers from the RO ray perigee relative to the Earth's (or planetary) surface. This implies the possibility of determining the position and orientation of the fronts of internal waves, which opens a new RO area in geophysical applications for remote sensing of the internal waves in the atmospheres and ionospheres of Earth and other planets (Gubenko et al., 2008a, b, 2011).

The goal of this paper is (i) to formulate a principle of locality; (ii) to present several important findings arising from the locality principle; and (iii) to introduce new index of ionospheric activity. The paper is structured as follows. In Sect. 2 the formulation of locality principle is presented. Section 3 describes three important findings following from the locality principle: (i) possibility to determine the total absorption at a single frequency; (ii) possibility to evaluate the height, displacement from the radio ray perigee, and tilt of the inclined ionospheric (atmospheric) layers; (iii) method for separation of the contributions of the layered and irregular structures in the RO signal and technique for measurement of parameters of layers and turbulence at a single frequency using joint analysis of the amplitude and phase variations. In Sect. 4 a new scintillation index based on the refractive attenuation found from the phase variations of the RO signal is introduced and its correlation with the S4 index is established. Conclusions are given in Sect. 5.

2 Principle of locality

The principle of locality is based on a previously established connection (Liou and Pavelyev, 2006; Liou et al., 2007; Pavelyev et al., 2008a, b, 2009, 2010a, b), which relates the eikonal acceleration a and refractive attenuation $X_p{}'(t)$ of the RO signal emitted by a transmitter G and received by satellite L after passing through a spherically symmetric medium with a center of symmetry at point O' (Fig. 1):

$$1-X_p{}'(t)=m'a,\ a=\frac{d^2\Phi(t)}{dt^2}=\lambda\frac{dF_d(t)}{dt},\ m'=\frac{d_2{}'d_1{}'}{(d_1{}'+d_2{}')}(dp_s{}'/dt)^{-2};\ p_s{}'=|O'D'|;\Phi(t)=\int_G^L n(l)dl-R_0 \quad (1)$$

where λ is the length of radio waves; d_1', d_2', and R_0 are the distances along the straight lines GD', $D'L$ and GL, respectively; D' is the projection of the center of symmetry O' onto the line GL; p_s' is the impact parameter of the straight line GL relative to the center O'; $\Phi(t)$ is the difference between the eikonal of radio waves propagating along the trajectory GTL and the length GL as a function of time t; $n(l)$ is the refractive index; dl is the differential length of the radio ray GTL; and the point T is the radio ray perigee relative to the Earth's surface having the altitude h (Fig. 1). Another important geometric parameter is the height H of the line of sight GDL above the surface. Point D is the projection of the center O on the straight line GL (Fig. 1). During a RO event the magnitude H changes from positive to negative values. The eikonal acceleration a (Eq.1) is proportional to the time derivative of the Doppler frequency of radio waves $F_d(t)$. Eq.1 is fulfilled under the following conditions (Liou et al., 2007; Pavelyev et al., 2008a, b):

$$\begin{aligned} &\left| p' - p_s' \frac{dR_{1,2}'}{dt} \right| \ll \left| p_s' \frac{dp_s'}{dt} \right|;\ d_1' \gg d_2'; \\ &\left| p' - p_s' \frac{d}{dt}\left(\frac{\partial \theta'}{\partial p_s'} \frac{dp_s'}{dt} \right) \right| \ll \left| \left(\frac{dp'}{dt} - \frac{dp_s'}{dt} \right) \frac{\partial \theta'}{\partial p_s'} \frac{dp_s'}{dt} \right| \end{aligned} \qquad (2)$$

where p' is the impact parameter of the ray GTL relative to the center O'; d_1', and d_2' are the distances GD', $D'L$, respectively; point D' is projection of the center of spherical symmetry O' on the line of sight GL. In the case of the RO ionospheric research the center of spherical symmetry can be shifted relative to the center O, and the first and third conditions (Eq. 1) are satisfied only if the distance OO' is significantly less than the Earth's radius ρ_e (Fig. 1). The second inequality (Eq. 2) is necessary for excluding the uncertainty because of symmetry of the coefficient m' with respect to variables d_2', d_1'. Inequalities (Eq. 2) are satisfied in the case of circular orbits of the satellites G and L at GPS RO atmospheric sounding, when the center of spherical symmetry O' is almost identical to the center of Earth (or planet) O, and the point T' coincides with the perigee T of the ray GTL (Fig. 1). Location of the radio ray perigee T in accordance with solution of the RO inverse problem determines the temporal dependencies of the height h above the Earth's surface and horizontal coordinates of the atmospheric layers (Melbourne et al, 1994; Melbourne, 2004; Yakovlev, 2002).

When absorption is absent, the refractive attenuation $X_p'(t)$ found from (Eq. 1) should be equal to the refractive attenuation $X_a(t)$ determined using the RO amplitude data (Liou and Pavelyev, 2006):

$$X_p'(t) \equiv X_a(t)\,;\, X_a(t) = I / I_0 \quad (3)$$

where I_0 and I are the intensities of the RO signal before and after the moment when the radio ray enters the medium, respectively. Identity (Eq. 3) is fulfilled if the coefficient m' in Eq. (1) is evaluated in accordance with location of the tangential point T', which is the perigee of radio ray GTL relative to the center of symmetry O', (Pavelyev et al., 2013). The refractive attenuation $X_a(t)$ measured from the RO intensity data does not depend on position of the point T' on the ray GTL and, naturally, on coefficient m'. The calculated value of the refractive attenuation $X_p'(t)$ does depend on the coefficient m' (Eq. 1) and location of the tangent point T' on the ray GTL. This permits to formulate the principle of locality under the conditions of single ray radio wave propagation and absence of absorption (Pavelyev et al., 2012, 2013; Pavelyev 2013): the refractive attenuations $X_p'(t)$ and $X_a(t)$ are equal if evaluation of $X_p'(t)$ is provided with the coefficient m' corresponding to the locations of the spherical symmetry centre O' and ray perigee T'**.** In accordance with the locality principle, the amplitude and phase variations of the radio waves registered at the point L may be considered as connected with influence of a small neighborhood of the ray perigee T' corresponding to the spherical symmetry centre O'.

3 Consequences of the locality principle

Next important findings follow from the locality principle.

3.1 Possibility of determination of the total absorption

If location of the symmetry center is known (for example, when the point O' coincides with the Earth's center O), the total absorption Γ in the atmosphere (ionosphere) can be defined by eliminating from the value $X_a(t)$ the refractive attenuation $X_p(h)$ found from the eikonal variations.

$$\Gamma = 10\lg\frac{X_a(t)}{X_p(t)} \quad (4)$$

Some results of determination of the refractive attenuations $X_a(h)$, $X_p(h)$, and total absorption Γ are considered below. Figure 2 (left and right plots) shows two vertical profiles of the refractive attenuations $X_a(h)$ and $X_a(h)$ highlighted by indices "*a*" and "*p*" (rough curves), respectively, and their polynomial approximation (smooth curves) measured at the first GPS frequency F1. The measurements were provided above two regions located in the Central Africa in 2008 (RO events October 18 17 h 52 m UT (left), and April 11 03 h 14 m UT (right), with geographical coordinates 5.0 N 332.5 W, and 6.7 N 328.1 W, respectively) using the FORMOSAT-3 satellites. The altitude dependences of $X_a(h)$ and $X_p(h)$ and their polynomial approximations are described by corresponding pairs of rough and smooth curves indicated by indices "*a*" and "*p*", respectively. The values of the altitudes of the line of sight $\mathrm{GDL}\,H$ and the height of the ray perigee h are plotted on the horizontal axis. The $X_a(h)$ and $X_p(h)$ profiles and their polynomial approximations are almost coincident at heights between 12 and 40 km, and significantly different below 8-9 km (Fig. 2, right and left plots). The correlation between variations of $X_a(h)$ and $X_p(h)$ gradually decreases with height H and magnitude of $X_a(h)$ is obviously well below the corresponding values of $X_p(h)$ in the 5-9 km altitude interval h. This indicates a possible influence of the total absorption of the radio waves in the atmosphere.

Other results obtained from the RO experiments carried out during four events on June 5, 2008, are shown in Fig. 3 (right part, groups of curves I-IY) and correspond to measurements of the refractive attenuations $X_p(h)$ and $X_a(h)$ at GPS frequency F1. These RO experiments were conducted in the following areas: Norwegian Sea (I), East Siberian Plateau (II), and South (III) and Central (IY) Alaska. The time and geographical coordinates of these RO events are: 16 h 18 m UT; 70.8 N 1.7 W (curves I); 13 h 28 m UT; 60.6 N 252.5 W (curves II); 02 h 42 m UT; 64.9 N 139.7 W (curves III); and 10 h 44 m UT; 60.0 N 155.8 W (curves IY). A weak but perceptible absorption in 1 db – 2 db interval at frequency F1 is observed below 8 km altitude. However, the altitude dependence of absorption Γ is very different in the considered regions. Two cases revealed significant decrease of absorption Γ in the 5 - 6 km (IY) and 7 - 8 km (II) height interval. In the remaining areas the total absorption changes from 1.5 db (I) up to 3.5 db (III) below 7 km altitude h.

Relevant to four RO events polynomial approximations of the measured at frequency F1 refractive attenuation $X_a(h)$, evaluated from the eikonal data at frequencies F1, F2 refractive attenuations $X_{p1}(h), X_{p2}(h)$, and estimated from the combined eikonal Φ_0 $\Phi_0 = (F_1^2\Phi_1 - F_2^2\Phi_2)/(F_1^2 - F_2^2)$ refractive attenuation $X_{p0}(h)$ are shown in Fig. 4. The measurement sessions correspond to four equatorial regions located in the Central Africa. Figure 4 (left plot) shows vertical profiles of the FORMOSAT-3 satellites found from data of four RO events carried out on April 2008 11 03 h 14 m UT, 6.7 N 328.1 W; May 29 21 h 41 m UT 3.1 N 329.5 W; October 11 0 h 56 m UT, 5.7 N 333.4 W; and October 18 17 h 52 m UT, 5.0 N 332.5 W; (curves 1–4, respectively). The values of the altitudes h of the ray perigee T and the height H of the straight line GL relative to the Earth' surface are marked on the horizontal axis. The $X_a(h)$ and $X_p(h)$ profiles are marked by indices "*a*" and "*p*", respectively. All three curves $X_p(h) = X_{p1}(h), X_{p2}(h), X_{p0}(h)$ are coincident in Fig. 4 (left plot). However, some distinction is seen in the right part of Fig. 4, where the altitude dependence of the total absorption is shown. This may be connected with influence of the ionosphere. The measured values of the total absorption coincide with a mean value of Γ equal to 0.0096$\pm$0.0024 db km^{-1} and correspond to the RO MIR–geostationary satellites data at the 32 cm wavelength (Pavelyev et al., 1996).

3.2 Determination of the tilt, height, and displacement of the inclined layers

If center of symmetry does not coincide with the expected location – point O, the principle of locality states:

$$X_a(t) \equiv X_p{}'(t);\ 1 - X_a(t) = m'a = \frac{m'}{m}\left[1 - X_p(t)\right] \tag{5}$$

where magnitudes of the refractive attenuation $X_p(t)$ and coefficient m correspond to position of the point O. Using relationship (Eq. 1) connecting coefficient m' with the distances d_1', d_2' and impact parameter p_s', one can obtain

$$\frac{m'}{m} - 1 = \frac{d_2' d_1' (dp_s / dt)^2}{d_2 d_1 (dp_s' / dt)^2} - 1; \; d_1 + d_2 = d_1' + d_2' = R_0 \tag{6}$$

If the displacement of spherical symmetry center satisfies the following conditions:

$$\frac{dp_s}{dt} \approx \frac{dp_s'}{dt}; \; \frac{d_2}{R_0} \ll 1; \; \frac{d_2'}{R_0} \ll 1 \tag{7}$$

one can find from (6), (7):

$$X_p(t) - X_a(t) = \frac{d_2' - d_2}{d_2}\left[1 - X_p(t)\right] = \frac{d}{d_2}\left[1 - X_p(t)\right] \tag{8}$$

where d is the distance DD' (see Fig. 1). It follows from Eqs. (5), (8) that amplitudes A_a, A_p of variations of the refractive attenuations $1 - X_a(h)$, $1 - X_p(h)$ and distance d are connected by equations:

$$m' = \frac{A_a(t)}{A_p(t)} m; \; d = \left[\frac{A_a(t)}{A_p(t)} - 1\right] d_2 \tag{9}$$

The coefficients m, m' are slowly changing as functions of time. Therefore the coefficient m' and layer's displacement d can be estimated in the time instant when the amplitude $A_p(t)$ achieves maximal magnitude. This allows finding, if absorption is absent, the displacement d of the tangential point T' with respect to the ray perigee T (Fig. 1) as well as the layer's height h' and inclination δ from following equations:

$$d = d_2' - d_2 = d_2 \;\; \alpha - 1 \; ; \; \alpha = \frac{A_a}{A_p}; \; d_2 = \sqrt{R_L^2 - p_s^2}, \; h' = h + \Delta h, \; \Delta h = \frac{r_e \delta^2}{2}, \; \delta = \frac{d}{r_e}, \; r_e = |TO|. \tag{10}$$

The amplitudes A_a, A_p of variations of the refractive attenuations $1 - X_a(h)$ and $1 - X_p(h)$, can be evaluated, for example, using the Hilbert numerical transform. The amplitude $A_p(t)$ of refractive attenuation $X_p(t)$ is evaluated using the coefficient m

corresponding to the centre of Earth (or planet) O. Depending on the sign of the difference $A_a - A_p$, the value of d is positive (or negative), and the point T' is located on the GT or TL lines, respectively. Note that relationship (Eq. 9) is fulfilled if one of the satellites is much farther away from the center of symmetry than the other. This condition is usually satisfied during the Earth or planetary RO missions (Fjeldbo, 1964; Yakovlev, 2002).

The spherical symmetry of a medium with new center O' justifies application of the Abel transformation for solution of the inverse problem (Pavelyev et al, 2008a, b). The time derivative of the phase path excess $\Phi(t)$ is used to obtain the temporal dependence of the impact parameter p':

$$p' - p_s' = -m' \frac{d\Phi}{dt}\frac{dp_s}{dt} = -m\alpha \frac{d\Phi}{dt}\frac{dp_s}{dt} = \alpha \;\; p - p_s \;\; . \tag{11}$$

To solve the inverse problem, the following formulas are used for the Abel transform (Hocke, 1997; Pavelyev et al., 2012a, b) (for simplicity, the bar in the designation of the impact parameters p', p_s' is deleted):

$$N(p) = -\frac{1}{\pi}\int_p^\infty \ln\left(\frac{x}{p} + \sqrt{\frac{x^2}{p^2} - 1}\right)\frac{d\xi(x)}{dx}dx \tag{12}$$

where p is the impact parameter corresponding to ray GTL in the instant of time t and $N(p)$ is the refractivity. The vertical gradient of the refractivity $dN(p)/dh$ can be found from Eq. (12) using a relationship:

$$\frac{dN(p)}{dh} = \frac{1 + N(p)}{1 - \frac{dN(p)}{dp} r_T}\frac{dN(p)}{dp} \tag{13}$$

where r_T is the distance $T'O'$ (Fig. 1). The derivative of the bending angle $\xi(p)$ on the impact parameter p can be found from the RO signal amplitude or the RO phase path excess data (Pavelyev et al., 2012, 2013), i.e.:

$$X(p)=\frac{p}{p_s\left|1-\sqrt{R_2^2-p^2}\sqrt{R_1^2-p^2}\,\frac{d\xi(p)}{dp}R_0^{-1}\right|};$$

$$\frac{d\xi(p)}{dp}=\ 1-p_s p^{-1}X^{-1}\ \ \frac{R_0}{\sqrt{R_2^2-p^2}\sqrt{R_1^2-p^2}}\approx\frac{1-X^{-1}\ \ R_0}{\sqrt{R_1^2-p^2}\sqrt{R_2^2-p^2}} \qquad (14)$$

The last equation Eq. (14) for $d\xi(p)/dp$ is valid under condition: $p\approx p_s$. Substitution Eq. (14) in Eq. (12) gives with accounting for relation $\frac{dp}{dt}=X(p)\frac{dp_s}{dt}$ (Kalashnikov et al., 1986):

$$N(p)=\frac{1}{\pi}\int_{-\infty}^{t(p)}\ln\left(\frac{x}{p}+\sqrt{\frac{x^2}{p^2}-1}\right)\frac{X(t)-1\ R_0}{\sqrt{R_1^2-x(t)^2}\sqrt{R_2^2-x(t)^2}}\frac{dp_s(t)}{dt}dt;$$
$$x(t)=p(t);-\infty<t\le t(p) \qquad (15)$$

From Eqs. (4), (20), and (21), one can obtain a modernized formula for the Abel inversion, i.e.,

$$N(p)=-\frac{1}{\pi}\int_{-\infty}^{t(p)}\ln\left(\frac{x}{p}+\sqrt{\frac{x^2}{p^2}-1}\right)\frac{m'aR_0}{\sqrt{R_1^2-x(t)^2}\sqrt{R_2^2-x(t)^2}}\frac{dp_s(t)}{dt}dt;$$
$$x(t)=p(t);-\infty<t\le t(p) \qquad (16)$$

where m' can be determined from the first equation Eq. (9).

When position of the spherical symmetry center is known (for example, a center of symmetry coincides with the center of the Earth), Eqs. (15) and (16) are new relationships for solution of the RO inverse problem. Unlike previous solution (Eq. 12), the Eqs. (15) and (16) do not contain the angle of refraction, and include only temporal dependences of the refractive attenuation $X(t)$, eikonal acceleration, and impact parameter. Note that Eqs. (15) and (16) provide the Abel transform in the time domain where a layer contribution does exist. The linear part of the regular trend due to the influence of the upper ionosphere is removed because the eikonal acceleration a in Eq. (16) contains the second derivative on time. However, the influence of the upper ionosphere is existing because it may contribute in the impact parameter $p(t)$. Also, the nonlinear contribution of the upper ionosphere remains in the eikonal acceleration a. Therefore, Eq. (16) approximately gives that part of the refractivity altitude distribution, which is connected with the influence of a sharp plasma layer. The electron density vertical distribution in the Earth's ionosphere $N_e(h)$ is connected at GPS frequencies with the refractivity $N(h)$ via the following relationship:

$$N_e(h) = -\frac{N(h)}{40.3} f^2 \qquad (17)$$

where f is the carrier frequency [Hz], and $N_e(h)$ is the electron content $[el/m^3]$.

Examples of application of Eqs. (12)–(16) for estimation of the location, inclination, and real height of ionospheric layers are given in Fig. 5. To consider a possibility to locate the plasma layers, a CHAMP RO event 026 (July 04, 2003, 02 h 27 m UT; geographic coordinates 68.5 N 82.8 W) with strong quasi-regular amplitude and phase variations is used. The refractive attenuations of the CHAMP RO signals $X_a(h)$, $X_p(h)$ found from the RO signal intensity and eikonal data are shown in Fig. 5a as functions of the RO ray perigee altitude h. The eikonal acceleration a has been estimated by the double differentiation of a second-power least square polynomial over a sliding time interval $\Delta t =$ 0.5 s. This time interval approximately corresponds to the vertical size of the Fresnel zone of about 1 km since the vertical component of the radio ray was about 2.1 km/s. The refractive attenuation $X_p(h)$ is derived from the evaluated magnitude a using Eq. (1), and m value is obtained from the orbital data. The refractive attenuation $X_a(h)$ is derived from the RO amplitude data by a sliding least-square polynomial having the same power with averaging in the time interval of 0.5 s. In the altitude ranges of 50–60 and 75–85 km, the refractive attenuations variations $X_a(h)$ and $X_p(h)$ are strongly connected and may be considered as coherent oscillations caused by sporadic layers (Fig. 5a, curves 1 and 2). Using a Hilbert numerical transform, the amplitudes A_a, A_p of analytical signals related to $1-X_a(h)$ and $1-X_p(h)$ have been computed and are shown in Fig. 5b, curves 1 and 2, respectively. In the altitude range of 50–60 km, amplitudes A_a, A_p are nearly identical, but the magnitude of A_a is about 1.7 times below than that of A_p. Accordingly, displacement d found from Eq. (9) is negative, and a plasma layer is displaced from the RO ray perigee T in the direction to satellite L (see Fig.

1). A similar form of variations of the refractive attenuations $1-X_a(h)$ and $1-X_p(h)$ allows locating the detected ionospheric layer. Displacement d corresponding to a plasma layer recorded at the 51-km altitude of the RO ray perigee is shown in Fig. 5c. Curves 1 and 2 in Fig. 5c correspond to amplitudes A_a, A_p. Curve 3 describes the displacement d found using Eq. (9) from amplitudes A_a, A_p in the 50.7 – 51.4 km altitude interval. The changes in d are concentrated in the altitude range of −900 km to −950 km when the functions A_a, A_p vary near their maximal values of 0.75 and 1.36 in the ranges of $0.7 \le A_a \le 0.75$; $1.29 \le A_p \le 1.36$, respectively. The statistical error in the determination of ratio $\frac{A_a(t)}{A_p(t)}$ in Eq. (9) is minimal when $A_p(t)$ is maximal. If the relative error in the measurements of A_p is 5%, according to Fig. 5c, the accuracy in the estimation of d is about $\pm$120 km. The inclination of a plasma layer to a local horizontal direction δ calculated using Eq. (10) is approximately equal to $\delta = 8.2^\circ \pm 0.2^\circ$. The vertical gradient $\frac{dN_e(h)}{dh}$ of the electron density distribution $N_e(h)$ for the given RO event is shown in Fig. 5d. Curves 1 and 2 correspond to the vertical gradient $\frac{dN_e(h)}{dh}$ retrieved using Eqs. (12) and (16), respectively. Curve 3 is related to the vertical gradient $\frac{dN_e(h)}{dh}$ retrieved using the refractive attenuation $X_a(h)$ and formula (Eq. 15). The real altitude of the ionospheric layers is indicated on the horizontal axis in Fig. 5d. Two ionospheric layers are seen (curves 1, 2, and 3 in Fig. 5d). The first layer is located on line TL at the 110 to 120 km altitudes at a distance of 900 km from point T (Fig. 5d, left). The second layer is located near the RO perigee at the 95 to 105 km altitudes (Fig. 5d, right). From the comparison of the refractive variations $X_a(h)$ and $X_p(h)$ (Fig. 5a, curves 1 and 2) and the vertical gradients of the electron content (Fig. 5d), the width of the sporadic *E*-layers is nearly equal to the altitude interval of the intensity variations of RO signals. From Fig. 5d, the variations of the vertical gradient of the electron density are concentrated in interval $-0.4\cdot 10^6[elcm^{-3}km^{-1}]$ < $\frac{dN_e(h)}{dh} < 0.5\cdot 10^6[elcm^{-3}km^{-1}]$. These magnitudes of $N_e(h)$ are typical for sporadic *E*-layers (Kelley and Heelis, 2009). The height interval of the RO signal amplitude variations is nearly equal to the height interval of the variations in the electron density and its gradient. It follows that the standard definition of the perigee of the radio ray in the RO method as the minimal value of the distance to the surface of the ray path leads to an underestimation (bias) of layers altitude in the atmosphere (ionosphere) of Earth and planets. This error is zero for horizontal layers and increases with their inclination.

3.3 Separation of the layers and small-scale irregularities contributions in the RO signal

The principle of locality allows one to separate the contributions of layers and irregular inhomogeneities in the RO signal. According to Eq. (5), the coherent and incoherent components of the RO atmospheric signal $C(h), I(h)$ due to the layers and irregularities influence can be estimated as:

$$C(h) = \left[X_a(h) + X_p(h)\right]/2 - P(h);\; I(h) = \left[X_a(h) - X_p(h)\right]/2 \tag{18}$$

where $P(h)$ is the polynomial approximation describing the main atmospheric contribution in the RO signal. If location of the spherical symmetry center is known, $P(h)$ should be the same for the refractive attenuations $X_a(h)$, $X_p(h)$. Example of separation of the layers and inhomogeneities contributions in the RO signal is presented below. Figure 6 shows altitude dependences of the refractive attenuations $X_a(h)$, $X_p(h)$ for the CHAMP RO event April 07 2003 carried out at 02 h 34 m UT in the area with geographical coordinates 2.5 S 291.7 W. The vertical profiles of the refractive attenuations $X_a(h)$, $X_p(h)$ reveal the coherent variations of $X_a(h)$, $X_p(h)$ indicating contribution of the atmospheric layers (Fig. 6, left, top curves X_A, X_P displaced for comparison). Dotted curves in Fig. 6, left (displaced for comparison), describe the polynomial approximations $P(h)$ of the slow changing altitude dependences of $X_a(h)$, $X_p(h)$. The coherent and incoherent parts of the RO signal $C(h), I(h)$ are obtained using formulas (Eq. 18) as shown in the Fig. 6, left, bottom plot (curves 1 and 2, respectively). The intensity of the coherent component $C(h)$ by an order of magnitude prevails the corresponding value of $I(h)$, thus, indicating importance of the layers contribution in the RO signal. Usually this contribution is assigned to effects of the small-scale irregularities (Cornman et al., 2012). Analysis of spatial spectra of coherent and incoherent components is presented in the Fig. 6, right, top and bottom plots, respectively. The forms of spectra $C(h), I(h)$ are similar in the interval of the vertical periods greater than 1 km. In the interval below 1 km, the power degrees of the spectra inclination are different and equal to 3.7$\pm$0.2 and 2.1 $\pm$0.2 for components $C(h)$ and $I(h)$, respectively. This indicates a different origin of the components $C(h)$ and $I(h)$. The inclination of the $I(h)$ spectrum is nearly 8/3 which corresponds to contribution of the turbulent irregularities in variations of the RO signal intensity (Gurvich and Yakushkin, 2004). The value 3.7 corresponding to the coherent component $C(h)$ is near the inclination of spatial spectrum of anisotropic internal gravity waves according with theory developed by Gurvich and Chunchuzov (2008).

Parameters of coherent and incoherent components introduced in the Table 1 illustrate a possibility to separate the contributions of atmospheric layers and turbulent structures in the RO signal. The time and geographic coordinates are shown in the first two columns of Table 1. The rms deviations σ_A, σ_P of the refractive attenuations $X_a(h)$, $X_p(h)$ and dispersion of the components $C(h)$ and $I(h)$ σ_c, σ_{in} are presented in the next four columns. The altitude interval $h_b \div h_u$ of measurements of $\sigma_A, \sigma_P; \sigma_c, \sigma_{in}$; and correlation coefficient r_c between the refractive attenuations variations $X_A(h)$, $X_P(h)$ are indicated in the last two columns of Table 1. As a rule the rms deviation σ_c of the coherent component $C(h)$ is greater than that one of incoherent part $I(h)$ σ_{in} by a factor of 4-5. This indicates on the prevailing contribution of the atmospheric layers as compared with influence of the irregularities in the RO signal. High level of correlation r_c (in the interval 0.84-0.96) between the variations of the refractive attenuations $X_a(h)$, $X_p(h)$ indicates the practical and theoretical importance of the locality principle for separation of the atmospheric layers and irregularities in the RO signal at a single frequency.

4 Relationships between the eikonal variations and intensity scintillations index S4

According to locality principle, there can exist a global correlation between the phase and amplitude variations of the RO signal. Index S4 (I), as measured from intensity variations, should be correlated with index S4 (F), defined by the second derivative on time of the eikonal of the RO signal at GPS frequencies F1 and F2. According to the principle of locality in the case of spherical symmetric medium, there can exist the next connections:

$$S4(X_a) = \sqrt{\frac{\langle X_a^2 \rangle - \langle X_a \rangle^2}{\langle X_a \rangle^2}};\; S4(X_p) = \sqrt{\frac{\langle X_p^2 \rangle - \langle X_p \rangle^2}{\langle X_p \rangle^2}}; S4(X_a) \equiv S4(X_p) \quad (19)$$

Figures 7 and 8 show the results of correlation of index S4(I), defined by the variations of the intensity I at the frequency F1 with indices S4(F1), S4(F2) measured from the second derivative of the phase paths excess at frequencies F1, F2 during FORMOSAT-3 RO events held in January and February 2012. Circles in Figs. 7 and 8 correspond to the experimental values of index S4 (I) (vertical axis) and S4 (F1), S4(F2) (horizontal axis). The solid curves in Figs. 7 and 8 are regression lines and have been found by least squares method. The correlation coefficient of index S4(I) to S4(F1) and S4(F2) varies in the intervals 0.69 to 0.78 and 0.70 - 0.75, respectively. The correlation coefficient of index S4(I) with combined index [S4(F1)+S4(I)]/2 is very high and changes in the interval 0.91-0.97. Measured correlation values indicate a significant contribution of regular layered irregularities in the ionospheric variations of the amplitude and phase of the RO signals at frequencies F1, F2. High correlation between variations of the indices S4(I) and S4 (F1), S4(F2) indicates substantially lower influence of the small-scale irregularities on the RO signal as compared with the contribution of the layered structures in the ionosphere.

5 Conclusions

The principle of locality is a key regularity that extends applicable domain of the RO method, widens possibilities and opens new directions of the RO geophysical applications to remote radio sensing the atmosphere and ionosphere of the Earth and planets. These directions includes: (i) innovative estimating the altitude dependence of the total absorption of radio waves using the RO amplitude and phase variations at a single frequency; (ii) evaluation of the slope, altitude, and horizontal displacement of the atmospheric and ionospheric layers from the RO amplitude and phase data using the eikonal acceleration/intensity technique; (iii) separation of layers and irregularities contributions in the RO signal, determination of vertical profiles of the turbulent and small-scale structures by joint analysis of the RO eikonal and amplitude variations; and (iv) introduction of the new combined phase-intensity index for the RO study of multilayered structures and wave processes. This regularity is valid for every RO ray trajectory in geometrical optics approximation including reflections from the surface.

Mass-scale measurements of the total absorption at the altitude below 15 km depend on the quality of the GPS receivers onboard of the RO missions. The total absorption measurements are possible only in the case when the low and high frequency noise are small enough for coinciding of the approximating the RO amplitude and phase data polynomials at the altitudes between 15 – 60 km. Also the stability of the RO phase data and accuracy of the total absorption measurements are determined by precision of the open-loop regime of the GPS RO receivers below 8 km altitude. Analysis of these technological aspects of the RO measurements is the task of future works.

It follows from Sect. 3.2 that the standard definition of the perigee of the radio ray in the RO method as the minimal value of the distance to the surface of the ray path leads to an underestimation (bias) of layers altitude in the atmosphere (ionosphere) of Earth and planets. This systematic bias is zero for horizontal layers and strongly increases with their inclination in the range 1-10 degrees from 1 km up to values about of several tens kilometers. The measured inclination of layers can be applied for estimating the orientation of wave's fronts in the ionosphere (or atmosphere) and may be used for determination of the important parameters of internal waves including the internal frequency, direction of kinetic momentum and others. The new method of estimating the electron density distribution in the plasma layers (described in Sect. 3.2) should be a subject of future comparison with the ionosondes and tomographic data.

Mass-scale measurements of coherent and incoherent component of the RO signal (Sect. 3.3) and introduced (Sect. 4) combined phase-intensity ionospheric index are important for investigation of the temporal, seasonal and regional evolution of the layered and turbulent structures at different altitudes in the ionosphere and atmosphere with a global coverage and can be provided in near future with usage of the extended volume of the RO data obtained during twenty years (1995-2015) of experimental researches.

Acknowledgements. We are grateful to Taiwan Center for Space and Remote Sensing Re-search for access to the FORMOSAT-3 RO data. This work was supported in part by Program no. 22 of the Presidium of the Russian Academy of Sciences, by the Fundamental Research, Program of the Physical Sciences Division of the Russian Academy of Sciences, IV.13 and Russian Foundation of Basic Research grant No. 13-02-00526-a. We are grateful to Dr. R. R. Salimzjanov for help in preparing the manuscript.

References

Anthes, R. A.: Exploring Earth’s atmosphere with radio occultation: contributions to weather, climate and space weather, Atmos. Meas. Tech., 4, 1077–1103, doi:10.5194/amt-4-1077-2011, 2011.

Arras, C., Wickert, J., Jacobi, Ch., Heise, S., Beyerle, G., and Schmidt, T.: A global climatology of ionospheric irregularities derived from GPS radio occultation, Geophys. Res. Lett., 35, L14809, doi:10.1029/2008GL034158, 2008.

Arras, C., Jacobi, C., Wickert, J., Heise, S., and Schmidt, T.: Sporadic E signatures revealed from multi-satellite radio occultation measurements, Adv. Radio Sci., 8, 225–230, doi:10.5194/ars-8-225-2010, 2010.

Bai, W. H., Sun, Y. Q., Du, Q. F., Yang, G. L., Yang, Z. D., Zhang, P., Bi, Y. M., Wang, X. Y., Cheng, C., and Han, Y.: An introduction to the FY3 GNOS instrument and mountain-top tests, Atmos. Meas. Tech., 7, 1817–1823, doi:10.5194/amt-7-1817-2014, 2014.

Benzon, H.-H., Nielsen, A. S., and Olsen, L.: An atmospheric wave optics propagator – theory and application, DMI, Scientific Report 03-01, DMI, Copenhagen, Denmark, 1–96, DMI, available at: http://www.dmi.dk/fileadmin/Rapporter/SR/sr03-01.pdf, 2003.

Beyerle, G. and Hocke, K.: Observation and simulation of direct and reflected GPS signals in Radio Occultation Experiments, Geophys. Res. Lett., 28, 1895–1898, 2001.

Beyerle, G., Wickert, J., Galas, R., Hocke, K., Konig, R., Marquardt, C., Pavelyev, A. G., Reigber, C., and Schmidt, T.: GPS occultation measurements with GPS/MET and CHAMP, Taikiken Shinpojiumu, 15, 44–47, 2001.

Beyerle, G., Hocke, K., Wickert, J., Schmidt, T., and Reigber, C.: GPS radio occultations with CHAMP: a radio holographic analysis of GPS signal propagation in the troposphere and surface reflections, J. Geophys. Res., 107, 4802, doi:10.1029/2001JD001402, 2002.

Cornman, L. B., Goodrich, R. K., Axelrad, P., and Barlow, E.: Progress in turbulence detection via GNSS occultation data, Atmos. Meas. Tech., 5, 789–808, doi:10.5194/amt-5-789-2012, 2012.

Fjeldbo, G.: Bistatic-Radar Methods for Studying Planetary Ionospheres and Surfaces, Ph.D. thesis, Stanford University, USA, 1964.

Fjeldbo, G., Kliore, A. J., and Eshleman, V. R.: The neutral atmosphere of Venus as studied with the Mariner V radio occultation experiments, Astron. J., 76, 123–140, 1971.

Foelsche, U., Kirchengast, G., Steiner, A. K., Kornblueh, L., Manzini, E., and Bengtsson, L.: An observing system simulation experiment for climate monitoring with GNSS radio occultation data: Setup and test bed study, J. Geophys. Res., 113, D11108, doi:10.1029/2007JD009231, 2008.

Fong, C.-J., Shiau, W.-T., Lin, C.-T., Kuo, T.-C., Chu, C.-H., Yang, S.-K., Nick, L. Y., Chen, S.-S., Kuo, Y.-H., Liou, Y.-A., and Chi, S.: Constellation deployment for the FORMOSAT-3/COSMIC mission, IEEE T. Geosci. Remote Sens., 46, 3367–3379, 2008.

Gorbunov, M. E.: Ionospheric correction and statistical optimization of radio occultation data, Radio Sci., 37, 17-1–17-9, 2002a.

Gorbunov, M. E.: Canonical transform method for processing GPS radio occultation data in lower troposphere, Radio Sci., 37, 9-1–9-10, doi:10.1029/2000RS002592, 2002b.

Gorbunov, M. E. and Gurvich, A. S.: Microlab-1 experiment: multipath effects in the lower troposphere, J. Geophys. Res., 103, 13819–13826, 1998a.

Gorbunov, M. E. and Gurvich, A. S.: Algorithms of inversion of Microlab-1 satellite data including effects of multipath propagation, Int. J. Remote Sens., 19, 2283–2300, 1998b.

Gorbunov, M. E. and Kirchengast, G.: Processing X/K Band Radio Occultation Data in Pres-ence of Turbulence, Radio Sci., 40, RS6001, doi:10.1029/2005RS003263, 2005.

Gorbunov, M. E. and Lauritsen, K. B.: Analysis of wave fields by Fourier integral operators and its application for radio occultations, Radio Sci., 39, RS4010, doi:10.1029/2003RS002971, 2004.

Gorbunov, M. E., Gurvich, A. S., and Bengtsson, L.: Advanced Algorithms of Inversion of GPS/MET Satellite Data and Their Application to Reconstruction of Temperature and Humidity, report No. 211, Max-Planck-Institute for Meteorology, Hamburg, 40 pp., 1996.

Gorbunov, M. E., Gurvich, A. S., and Shmakov, A. V.: Back-propagation and radio-holographic methods for investigation of sporadic ionospheric E-layers from Microlab-1 data, Int. J. Re-mote Sens., 23, 675–685, 2002.

Gorbunov, M. E., Lauritsen, K. B., and Leroy, S. S.: Application of Wigner distribution function for analysis of radio occultations, Radio Sci., 45, RS6011, doi:10.1029/2010RS004388, 2010.

Gubenko, V. N., Andreev, V. E., and Pavelyev, A. G.: Detection of layering in the upper cloud layer of Venus northern polar atmosphere observed from radio occultation data, J. Geophys. Res., 113, E03001, doi:10.1029/2007JE002940, 2008a.

Gubenko, V. N., Pavelyev, A. G., and Andreev, V. E.: Determination of the intrinsic frequency and other wave parameters from a single vertical temperature or density profile measurement, J. Geophys. Res., 113, D08109, doi:10.1029/2007JD008920, 2008b.

Gubenko, V. N., Pavelyev, A. G., Salimzyanov, R. R., and Pavelyev, A. A.: Reconstruction of internal gravity wave parameters from radio occultation retrievals of vertical temperature pro-files in the Earth's atmosphere, Atmos. Meas. Tech., 4, 2153–2162, doi:10.5194/amt-4-2153-2011, 2011.

Gurvich, A. S. and Chunchuzov, I. P.: Model of the Three-Dimensional Spectrum of Anisotropic Temperature Irregularities in a Stably Stratified Atmosphere, Izv. Atmos. Ocean. Phys., 44, 567–582, 2008.

Gurvich, A. S. and Krasil'nikova, T. G.: Navigation satellites for radio sensing of the Earth's atmosphere, Sov. J. Remote Sens., 6, 89–93, 1987 (in Russian), 6, 1124–1131, 1990 (in English).

Gurvich, A. S. and Yakushkin, I. G.: Observation of quasi-periodical structures in the strato-sphere from space, Izv. Atmos. Ocean. Phys., 40, 737–746, 2004.

Hajj, G. A. and Romans, L. J.: Ionospheric electron density profiles obtained with the Global Positioning System: results from GPS/MET experiment, Radio Sci., 33, 175–190, 1998.

Hajj, G. A., Ao, C. O., Iijima, B. A., Kuang, D., Kursinski, E. R., Mannucci, A. J., Meehan, T. K., Romans, L. J., de la Torre Juarez, M., and Yunck, T. P.: CHAMP and SAC-C atmospheric occultation results and intercomparisons, J. Geophys. Res., 109, D06109,doi:10.1029/2003JD003909, 2004.

Hinson, D. P., Flasar, F. M., Schinder, A., Twicken, J. D., and Herrera, R. G.: Jupiter's iono-sphere: results from the first Galileo radio occultation experiment, Geophys. Res. Lett., 24, 2107–2110, 1997.

Hinson, D. P., Simpson, R. A., Twicken, J. D., Tyler, G. L., and Flasar, F. M.: Initial results from radio occultation measurements with Mars Global Surveyor, J. Geophys. Res., 104, 26997–27012, 1999.

Hocke, K.: Inversion of GPS meteorology data, Ann. Geophys., 15, 443–450, doi:10.1007/s00585-997-0443-1, 1997.

Hocke, K., Pavelyev, A., Yakovlev, O., Barthes, L., and Jakowski, N.: RO data analysis by radio holographic method, J. Atmos. Sol.-Terr. Phys., 61, 1169–1177, 1999.

Igarashi, K., Pavelyev, A. G., Hocke, K., Kucherjavenkov, A. I., Matugov, S. S., Yakovlev, O. I., Pavelyev, D., and Zakharov, A.: Radio holographic principle for observing natural processes in the atmosphere and retrieving meteorological parameters from radio occultation data, Earth Planets Space, 52, 868–875, 2000.

Igarashi, K., Pavelyev, A. G., Hocke, K., Pavelyev, D., and Wickert, J.: Observation of wave structures in the upper atmosphere by means of radio holographic analysis of the RO data, Adv. Space Res., 27, 1321–1327, 2001.

Jensen, A. S., Lohmann, M., Benzon, H.-H., and Nielsen, A. S.: Full spectrum inversion of radio occultation signals, Radio Sci., 38, 1040, doi:10.1029/2002RS002763, 2003.

Jensen, A. S., Lohmann, M., Nielsen, A. S., and Benzon, H.-H.: Geometrical optics phase matching of radio occultation signals, Radio Sci., 39, RS3009, doi:10.1029/2003RS002899, 2004.

Jakowski, N., Leitinger, R., and Angling, M.: Radio occultation techniques for probing the iono-sphere, Ann. Geophys.-Italy, 47, 1049–1066, 2004.

Joo, S., Eyre, J., and Marriott, R.: The Impact of METOP and Other Satellite Data Within the Met Offce Global NWP System Using an Adjoint-Based Sensitivity Method, Forecasting Research Technical Report no. 562, February, 1–18, 2012.

Kalashnikov, I. E., Matyugov, S. S., Pavelyev, A. G., and Yakovlev, O. I.: Analysis of the features of radio occultation method for the Earth's atmosphere study, in: The Book Electromagnetic Waves in the Atmosphere and Space, Nayka Ed., Moscow, 208–218, 1986 (in Russian).

Karayel, E. T. and Hinson, D. P.: Sub-Fresnel vertical resolution in atmospheric profiles from radio occultation, Radio Sci., 32, 411–418, 1997.

Kelley, M. C. and Heelis, R. A.: The Earth's Ionosphere: Plasma Physics and Electrodynamics, Elsevier Science, New York, 2009.

Kirchengast, G., Steiner, A. K., Foelsche, U., Kornblueh, L., Manzini, E., and Bengtsson, L.: Spaceborne climate change monitoring by GNSS occultation sensors, in: Proc. 11th Symp. Global Change Studies, AMS Ann. Meeting 2000, Long Beach, Calif., 62–65, 2000.

Kunitsyn, V. E. and Tereshchenko, E. D.: Ionospheric Tomography, Springer-Verlag, Berlin, 2003.

Kunitsyn, V. E., Nesterov, I., Padokhin, A., and Tumanova, Y.: Ionospheric radio tomography based on the GPS/GLONASS navigation systems, J. Commun. Technol. El., 56, 1269–1281, 2011.

Kunitsyn, V. E., Andreeva, E., Nesterov, I., and Padokhin, A.: Ionospheric sounding and tomog-raphy by GNSS, in: Geodetic Sciences – Observations, Modeling and Applications, chapter 6, edited by: Jin, S., InTech Publisher, ISBN 978-953-51-1144-3, 354 pp., doi:10.5772/3439, 2013.

Kursinski, E. R., Hajj, G. A., Schofield, J. T., Kursinski, E. R., Hajj, G. A., Schofield, J. T., Linfield, R. P., and Hardy, K. R.: Observing Earth's atmosphere with radio occultation measurements using the global positioning system, J. Geophys. Res., 102, 23429–23465, 1997.

Lindal, G. F., Wood, G. E., Hotz, H. B., Sweetnam, D. N., Eshleman, V. R., and Tyler, G. L.: The atmosphere of Titan: an analysis of the Voyager 1 radio occultation measurements, Icarus, 53, 348–363, 1983.

Lindal, G. F., Lyons, J. R., Sweetnam, D. N., Eshleman, V. R., Hinson, D. P., and Tyler, G. L.: The atmosphere of Uranus: results of radio occultation measurements with Voyager, J. Geophys. Res., 92, 14987–15001, 1987.

Liou, Y. A. and Pavelyev, A. G.: Simultaneous observations of radio wave phase and intensity variations for locating the plasma layers in the ionosphere, Geophys. Res. Lett., 33, L23102, 1–5, 2006.

Liou, Y.-A., Pavelyev, A. G., Huang, C.-Y., Igarashi, K., and Hocke, K.: Simultaneous obser-vation of the vertical gradients of refractivity in the atmosphere and electron density in the lower ionosphere by radio occultation amplitude method, Geophys. Res. Lett., 29, 43-1–43-4, 2002.

Liou, Y.-A., Pavelyev, A. G., Huang, C.-Y., Igarashi, K., Hocke, K., and Yan, S. K.: Analytic method for observation of the GW using RO data, Geophys. Res. Lett., 30, ASC 1-1–1-5, 2003.

Liou, Y. A., Pavelyev, A. G., Pavelyev, A. A., Wickert, J., and Schmidt, T.: Analysis of atmospheric and ionospheric structures using the GPS/MET and CHAMP radio occultation data base: a methodological review, GPS Solut., 9, 122–143, 2005.

Liou, Y. A., Pavelyev, A. G., Liu, S.-F., Pavelyev, A. A., Yen, N., Huang, C.-Y., and Fong, C.-J.: FORMOSAT-3/COSMIC GPS radio occultation mission: preliminary results, IEEE T. Geosci. Remote, 45, 3813–3826, 2007.

Liou, Y. A., Pavelyev, A. G., Matyugov, S. S., Yakovlev, O. I., and Wickert, J.: Radio Occultation Method for Remote Sensing of the Atmosphere and Ionosphere, edited by: Liou, Y. A., IN-TECH, In-The Olajnica 19/2, 32000 Vukovar, Croatia, 170, 45 pp., ISBN 978-953-7619-60-2, 2010.

Manzini, E. and Bengtsson, L.: An observing system simulation experiment for climate monitoring with GNSS radio occultation data: setup and test bed study, J. Geophys. Res., 113, D11108, 1–14, doi:10.1029/2007JD009231, 2008.

Marouf, E. A. and Tyler, G. L.: Microwave edge diffraction by features in Saturn's rings: observations with Voyager 1, Science, 217, 243–245, 1982.

Melbourne, W. G.: Radio Occultations Using Earth Satellites: A Wave Theory Treatment, Jet Propulsion Laboratory California Institute of Technology, Monograph

6, Deep Space Communications and Navigation Series, edited by: Yuen, J. H., the Deep Space Communications and Navigation Systems Center of Excellence Jet Propulsion Laboratory California Institute of Technology, 610 pp., 2004.

Melbourne, W. G., Davis, E. S., Duncan, C. B., Hajj, G. A., Hardy, K. R., Kursinski, E. R., Meehan, T. K., Young, L. E., and Yunck, T. P.: The application of spaceborne GPS to atmospheric limb sounding and global change monitoring, JPL Publication, 94-18, 147 pp., 1994.

Mortensen, M. D. and Høeg, P.: Inversion of GPS occultation measurements using Fresnel diffraction theory, Geophys. Res. Lett., 25, 2441–2444, 1998.

Mortensen, M. D., Lifield, R. P., and Kursinski, E. R.: Vertical resolution approaching 100m for GPS occultations of the Earth’s atmosphere, Radio Sci., 36, 1475–1484, 1999.

Pavelyev, A. G. and Kucherjavenkov, A. I.: Refractive attenuation in the planetary atmospheres, Radio Eng. Electron. P., 23, 13–19, 1978.

Pavelyev, A. G., Volkov, A. V., Zakharov, A. I., Krytikh, S. A., and Kucherjavenkov A. I.: Bistatic radar as a tool for Earth observation using small satellites, Acta Astronautica, 39, 721–730, 1996.

Pavelyev, A. G., Liou, Y.-A., Huang, C. Y., Reigber, C., Wickert, J., Igarashi, K., and Hocke, K.: Radio holographic method for the study of the ionosphere, atmosphere and terrestrial surface using GPS occultation signals, GPS Solut., 6, 101–108, 2002.

Pavelyev, A. G., Liou, Y. A., and Wickert, J.: Diffractive vector and scalar integrals for bistatic radio-holographic remote sensing, Radio Sci., 39, RS4011, 1–16, doi:10.1029/2003RS002935, 2004.

Pavelyev, A. G., Liou, Y. A., Wickert, J., Schmidt, T., Pavelyev, A. A., and Liu, S. F.: Effects of the ionosphere and solar activity on radio occultation signals: application to CHAllenging Minisatellite Payload satellite observations, J. Geophys. Res. 112, A06326, 1–14, 2007.

Pavelyev, A. G., Wickert, J., and Liou, Y.-A.: Localization of plasma layers in the ionosphere based on observing variations in the amplitude and phase of radiowaves along the satellite-to-satellite path, Radiophys. Quantum El., 51, 1–8, 2008a.

Pavelyev, A. G., Liou, Y.-A., Wickert, J., Pavelyev, A. A., Schmidt, T., Igarashi, K., and Matyugov, S. S.: Location of layered structures in the ionosphere and atmosphere by use of GPS occultation data, Adv. Space Res., 42, 224–228, 2008b.

Pavelyev, A. G., Liou, Y. A., Wickert, J., Gavrik, A. L., and Lee, C. C.: Eikonal acceleration technique for studying of the Earth and planetary atmospheres by radio occultation method, Geophys. Res. Lett., 36, L21807, 1–5, doi:10.1029/2009GL040979, 2009.

Pavelyev, A. G., Liou, Y.-A., Wickert, J., Schmidt, T., Pavelyev, A. A., and Matyugov, S. S.: Phase acceleration: a new important parameter in GPS occultation technology, GPS Solut., 14, 3–14, doi:10.1007/s10291-009-0128-1, 2010a.

Pavelyev, A. G., Liou, Y. A., Wickert, J., Zhang, K., Wang, C.-S., and Kuleshov, Y.: Analytical model of electromagnetic waves propagation and location of inclined plasma layers using occultation data, Prog. Electromagn. Res., 106, 177–202, doi:10.2528/PIER10042707, 2010b.

Pavelyev, A. G., Zhang, K., Matyugov, S. S., Liou, Y. A., Wang, C. S., Yakovlev, O. I., Kucherjavenkov, I. A., and Kuleshov, Y.: Analytical model of bistatic reflections and radio occultation signals, Radio Sci., 46, RS1009, doi:10.1029/2010RS004434, 2011a.

Pavelyev, A. G., Zhang, K., Wang, C. S., Kuleshov, Y., Liou, Y. A., and Wickert, J.: Identification of Inclined Ionospheric Layers Using Analysis of GPS Occultation Data, IEEE Transactions on Geoscience and Remote Sensing, 49, 6, 2374-2384 p. 10.1109/TGRS.2010.2091138, 2011b.

Pavelyev, A. G., Liou, Y. A., Zhang, K., Wang, C. S., Wickert, J., Schmidt, T., Gubenko V. N., Pavelyev, A. A., and Kuleshov, Y.: Identification and localization of layers in the ionosphere using the eikonal and amplitude of radio occultation signals, Atmos. Meas. Tech., 5, 1–16, doi:10.5194/amt-5-1-2012, 2012.

Pavelyev, A. A., Pavelyev, A. G., Matyugov, S. S., Yakovlev, O.I., Liou, Y. A., Zhang, K., and Wickertm J.: Radio Wave Propagation Phenomena from GPS Occultation Data Analysis, In the book Wave Propagation. Theories and Applications. Ed. By Yi Zheng. Chapter 5. Pp. 113-154. Published by InTech. Janeza Trdine 9, 51000 Rijeka, Chroatia. ISBN 978-953-51-0979-2. http://dx.doi.org/10.5772/3393. Copyright@2013 InTech.www.intechopen.com. 2013a.

Pavelyev, A. G.: The Principle of the Locality and Radio Occultation Method for Remote Sensing of Layers in the Atmosphere and Ionosphere on Earth and Other Planets, Doklady Physics, 58, pp. 375–378. PleiadesPublishing, Ltd. DOI: 10.1134/S1028335813090103. 2013.

Pavelyev, A. G., Zhang, K., Liou, Y. A., Pavelyev, A. A., Wang, C.-S., Wickert, J., Schmidt, T., and Kuleshov Y.: Principle of Locality and Analysis of Radio Occultation Data, IEEE Transactions on Geoscience and Remote Sensing, 51, 3240-3249, DOI 10.1109/TGRS.2012.22256292013, 2013b.

Rius, A., Ruffini, G., and Romeo, A.: Analysis of ionospheric electron density distribution from GPS/Met occultations, IEEE T. Geosci. Remote Sens., 36, 383–394, 1998.

Sokolovskiy, S. V.: Inversion of RO amplitude data, Radio Sci., 35, 97–105, 2000.

Sokolovskiy, S. V., Schreiner, W., Rocken, C., and Hunt, D.: Detection of high-altitude ionospheric irregularities with GPS/MET, Geophys. Res. Lett., 29, 621–625, 2002.

Steiner, A. K. and Kirchengast, G.: GW spectra from GPS/MET occultation observations, J. Atmos. Ocean. Tech., 17, 495–503, 2000.

Steiner, A. K., Kirchengast, G., and Ladreiter, H. P.: Inversion, error analysis, and validation of GPS/MET occultation data, Ann. Geophys., 17, 122–138, doi:10.1007/s00585-999-0122-5, 1999.

Steiner, A. K., Kirchengast, G., Foelsche, U., Kornblueh, L., Manzini, E., and Bengtsson, L.: GNSS occultation sounding for climate monitoring, Phys. Chem. Earth Pt. A, 26, 113–124, 2001.

Syndergaard, S.: Modeling the impact of the Earth’s oblateness on the retrieval of temperature and pressure profiles from limb sounding, J. Atmos. Sol.-Terr. Phy., 60, 171–180, 1998.

Syndergaard, S.: Retrieval analysis and methodologies in atmospheric limb sounding using the GNSS radio occultation technique, DMI Sci. Rep. 99-6, Danish Met. Inst., Copenhagen, Denmark, 131 pp., available at http://www.cosmic.ucar.edu/groupAct/references/Sr99-6.pdf (last access: 10 January 2015), 1999.

Von Engeln, A., Andresa, Y., Marquardt, C., Sancho, F.: GRAS Radio Occultation on-board of Metop, Adv. Space Res., 47, 336–347, doi:10.1016/j.asr.2010.07.028, 2011.

Vorob’ev, V. V. and Krasilnikova, T. G.: Estimation of accuracy of the atmosphere refractive index recovery from Doppler shift measurements at frequencies used in the NAVSTAR system, Izv. Russ. Acad. Sci., 29, 602–609, 1994 (Engl. Transl.).

Vorob'ev, V. V., Gurvich, A. S., Kan, V., Sokolovskiy, S. V., Fedorova, O. V., and Shmakov, A. V.: The structure of the ionosphere from theGPS-"Microlab-1" radio occultation data: preliminary results, Cosmic Res., 4, 74–83, 1997 (in Russian).

Ware, R., Exner, M., Feng, D., Gorbunov, M., Hardy, K., Herman, B., Kuo, Y.-H., Meehan, T., Melbourne, W., Rocken, C., Schreiner, W., Sokolovskiy, S., Solheim, F., Zou, X., Anthes, R., Businger, S., and Trenberth, K.: GPS soundings of the atmosphere from low earth orbit: preliminary results, B. Am. Meteorol. Soc., 77, 19–40, 1996.

Wickert, J., Pavelyev, A. G., Liou, Y. A., Schmidt, T., Reigber, C., Igarashi, K., Pavelyev, A. A., and Matyugov, S.: Amplitude scintillations in GPS signals as a possible indicator of iono-spheric structures, Geophys. Res. Lett., 31, L24801, 1–4, 2004.

Wickert, J., Reigber, C., Beyerle, G., Konig, R., Marquardt, C., Schmidt, T., Grunwaldt, L., Galas, R., Meehan, T. K., Melbourne, W. G., and Hocke, K.: Atmosphere sounding by GPS radio occultation: first results from CHAMP, Geophys. Res. Lett., 28, 3263–3266, 2001.

Wickert, J., Beyerle, G., König, R., Heise, S., Grunwaldt, L., Michalak, G., Reigber, Ch., and Schmidt, T.: GPS radio occultation with CHAMP and GRACE: a first look at a new and promising satellite configuration for global atmospheric sounding, Ann. Geophys., 23, 653–658, doi:10.5194/angeo-23-653-2005, 2005.

Wickert, J., Schmidt, T., Michalak, G., Heise, S., Arras, C., Beyerle, G., Falck, C., König, R., Pingel, D., and Rothacher, M.: GPS radio occultation with CHAMP, GRACE-A, SAC-C, TerraSAR-X, and FORMOSAT-3/COSMIC: brief review of results from GFZ, in: New Horizons in Occultation Research: Studies in Atmosphere and Climate, edited by: Steiner, A., Pirscher, B., Foelsche, U., and Kirchengast, G., Springer, 3–16, 2009.

Zus, F., Grunwaldt, L., Heise, S., Michalak, G., Schmidt, T., and Wickert, J.: Atmosphere sounding by GPS radio occultation: first results from TanDEM-X and comparison with TerraSAR-X, Adv. Space Res., 53, 272–279, doi:10.1016/j.asr.2013.11.013, 2014.

Yakovlev, O. I.: Space Radio Science, Taylor and Francis, London, 306 pp., 2003.

Yakovlev, O. I., Pavelyev, A. G., and Matyugov, S. S.: Radio Occultation Monitoring of the Atmo-sphere and Ionosphere, URSS Edition, Moscow, 206 pp., ISBN 978-5-397-01227-0, 2010 (in Russian).

Yunck, T. P., Lindal, G. F., and Liu, C.-H.: The role of GPS in precise Earth observation, in: Proc. IEEE Position Location and Navigation Symposium (PLANS 88), 29 November–December, 1988.

Yunck, T. P., Liu, C.-H., and Ware, R.: A history of GPS sounding, Terr. Atmos. Ocean. Sci., 11, 1–20, 2000.

Zhang, K., Zhang, S., Le Marshall, J., Kirchengast, G., Norman, R., Ying Li, Liu, C., and Carter, B.: A new Australian GNSS radio occultation data processing platform, in: IGNSS 2013 Symposium Proc., Gold Coast, Australia, ISBN 978-0-646-90640-9, Pap.85/12p., 2013.

TABLE 1. Parameters of coherent and incoherent components

Time (UT)	Location	σ_A	σ_P	σ_c	σ_{in}	$h_b \div h_u$, km	r_c
2003 04 17 21:38	58.9° N 117.5° E	0.084	0.062	0.071	0.018	12÷30	0.88
2003 04 17 22:05	45.8° S 146.9° E	0.07	0.058	0.062	0.015	14÷25	0.88
2003 04 17 23:13	48.7° N 124.4° E	0.11	0.097	0.104	0.022	12÷27	0.91
2003 04 26 00:06	55.8°N 74.2° E	0.065	0.052	0.056	0.016	11÷26	0.85
2003 04 26 00:13	31.1°N 74.6° E	0.051	0.036	0.042	0.011	18÷32	0.86
2003 04 26 01:21	51.8° N 125.2°W	0.096	0.076	0.085	0.015	12÷26	0.94
2003 04 26 01:23	58.1° N 92.8° W	0.055	0.039	0.046	0.011	13÷25	0.88
2003 04 26 04:42	65.3° N 35.3° E	0.056	0.043	0.048	0.014	10÷22	0.85
2003 05 03 00:34	0.4° S 63.0° E	0.11	0.086	0.096	0.027	17.5÷26	0.86
2003 05 03 01:27	22.2° N 121.6°W	0.14	0.11	0.123	0.023	12÷27	0.94
2003 05 03 03:35	12.6° N 38.6° E	0.079	0.065	0.071	0.012	20÷30	0.95
2003 05 03 04:56	59.4° N 17.0° E	0.05	0.039	0.043	0.011	12.5÷26.5	0.87
2003 04 12 07:48	45.6° S 7.6° E	0.066	0.047	0.056	0.012	14÷25	0.915
2003 04 12 08:25	7.4° N 153.9° E	0.103	0.076	0.088	0.013	18÷30	0.96
2003 04 12 08:53	57.5° N 42.2° W	0.06	0.052	0.055	0.011	12÷24	0.918
2003 04 12 09:37	70.8° S165.0° E	0.069	0.054	0.06	0.015	12÷22	0.88
2003 04 1210:08	52.2° N 150.9° E	0.085	0.069	0.075	0.016	12.5÷27	0.92

Figure captions

Figure 1. Scheme of radio occultation measurements.

Figure 2. Comparison of the refractive attenuations $X_a(h)$ and $X_p(h)$ and their polynomial approximations, corresponding to the FORMOSAT-3 RO measurements carried out on October 18 and April 11, 2008 (left and right plots, respectively). Thick and thin rough curves (marked by indices "*p*" and "*a*") describe the vertical profiles of $X_p(h)$ and $X_a(h)$, respectively. Smooth curves describing polynomial approximations of the altitudes dependences of $X_p(h)$ and $X_a(h)$ are also highlighted by indices "*p*" and "*a*".

.

Figure 3. Left plot. Comparison of the refractive attenuations $X_a(h)$ and $X_p(h)$ (groups of curves I-IY). Each group consists of four curves. In each group thick and thin rough curves (marked by indices "*p*" and "*a*") describe the experimental vertical profiles of $X_p(h)$ and $X_a(h)$, respectively. Smooth curves in each group describe polynomial approximations of the altitudes dependences of $X_p(h)$ and $X_a(h)$ and are also highlighted by indices "*p*" and "*a*", respectively. For convenience groups of curves II-IY are displaced by 0.6; 1.2; 1.8 units. Right. The total absorption Γ corresponding to the refractive attenuations $X_a(h)$, $X_p(h)$ measured at frequency F1 has been calculated from the smooth curves I-IY (marked by indices *a, p* in left panel). Curves II, III, and IY are shifted for comparison by 1, 2, and 3 db, respectively.

Figure 4. Left plot. Comparison of the polynomial approximations of refractive attenuations $X_a(h)$, $X_p(h)$ (curves 1-4, indexes "*p*" and "*a*", respectively). Curves 2-4 are displaced for convenience by 0.6; 0.4; 0.2, respectively. Right. The total absorption Γ corresponding to the refractive attenuations $X_a(h)$, $X_p(h)$ has been

calculated from the curves 1-4 (right panel). Curves 2, 3, and 4 are shifted for convenience by 2, 4, and 6 db, respectively.

Figure 5. a) Comparison of the refractive attenuations $X_a(h)$, $X_p(h)$ found from the RO intensity and eikonal data at GPS frequency F1 (curves 1 and 2, respectively). b) The amplitudes A_a, A_p of analytical signals corresponding to the variations of the refractive attenuations $1-X_a(h)$ and $1-X_p(h)$ (curves 1 and 2), respectively. c). Location of the first layer using amplitudes A_a, A_p. d). c) Vertical profiles of the gradients of electron density in the layers.

Figure 6. Left, top. Comparison of the refractive attenuations $X_a(h)$, $X_p(h)$ found from the RO intensity and eikonal data at GPS frequency F1 (curves X_A and X_P, respectively, displaced for comparison). Dotted curves show the polynomial approximations of the refractive attenuations $X_a(h)$, $X_p(h)$. Left, bottom. Contribution of the atmospheric layers (coherent component of the RO signal) and small scale irregularities (incoherent component) (curves 1 and 2, respectively). Right. Spatial spectra of the coherent and incoherent components of the RO signal (top and bottom panels, respectively).

Figure 7. Correlation of index S4(I) measured from the intensity variations of the GPS RO signal at frequency F1 and parameters S4(F1) and S4(F2) found from the eikonal variations at GPS frequencies F1 and F2.

Figure 8. Correlation of indices S4(I) and [S4(F1)+S4(I)]/2.

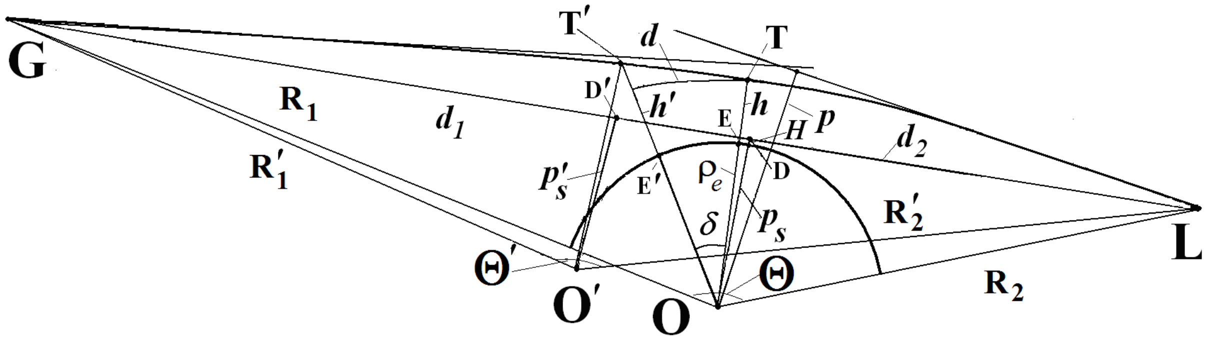

Fig. 1

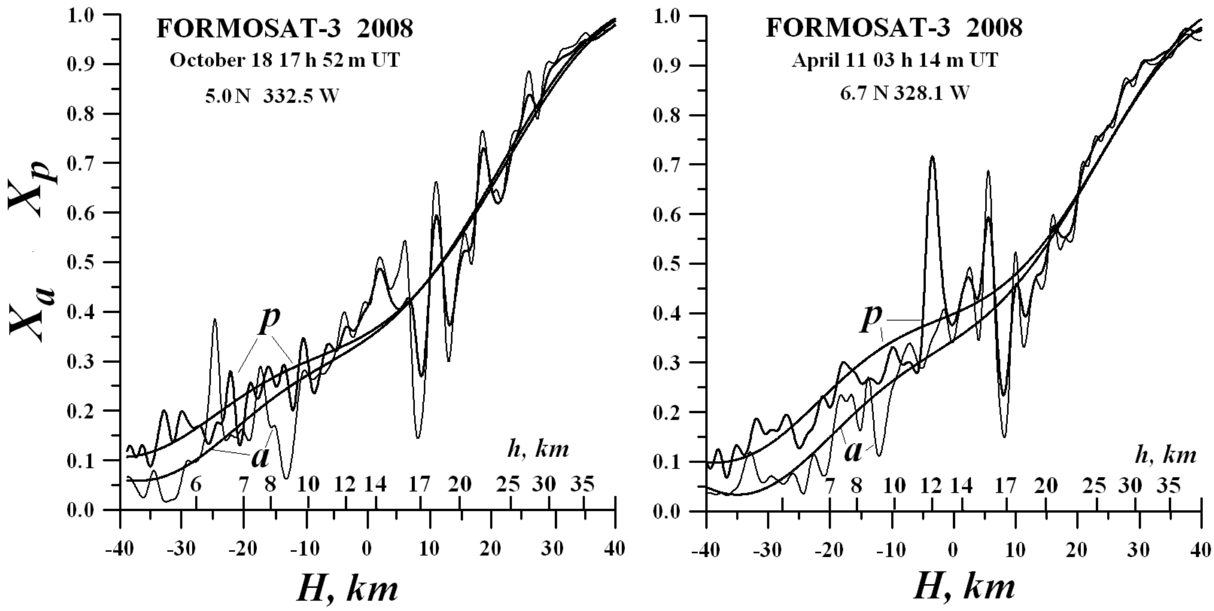

Fig.2

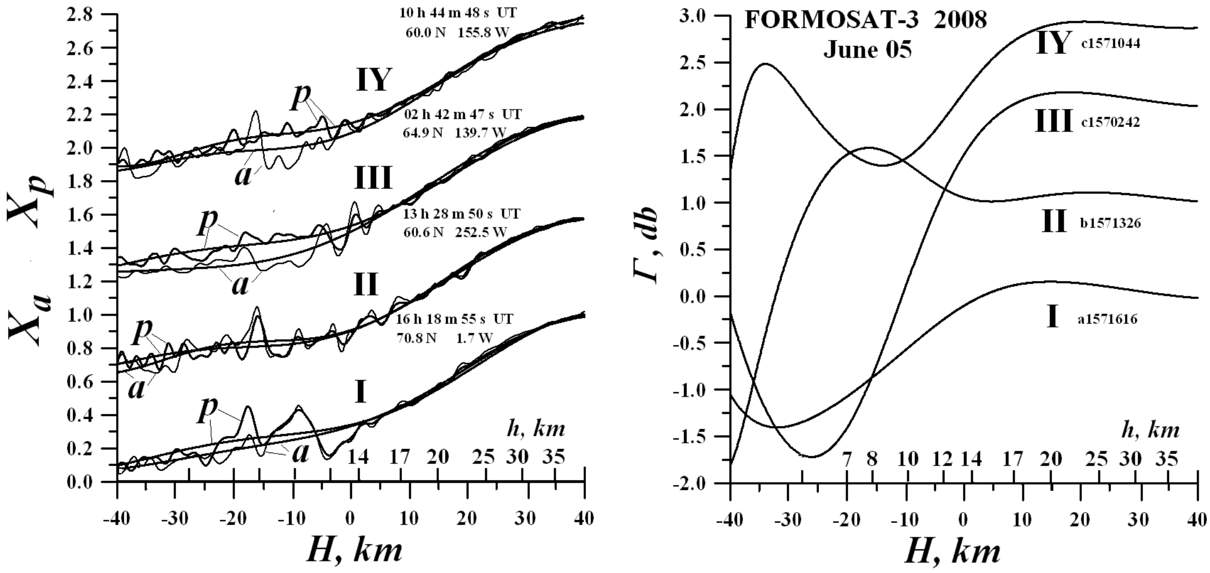

Fig. 3

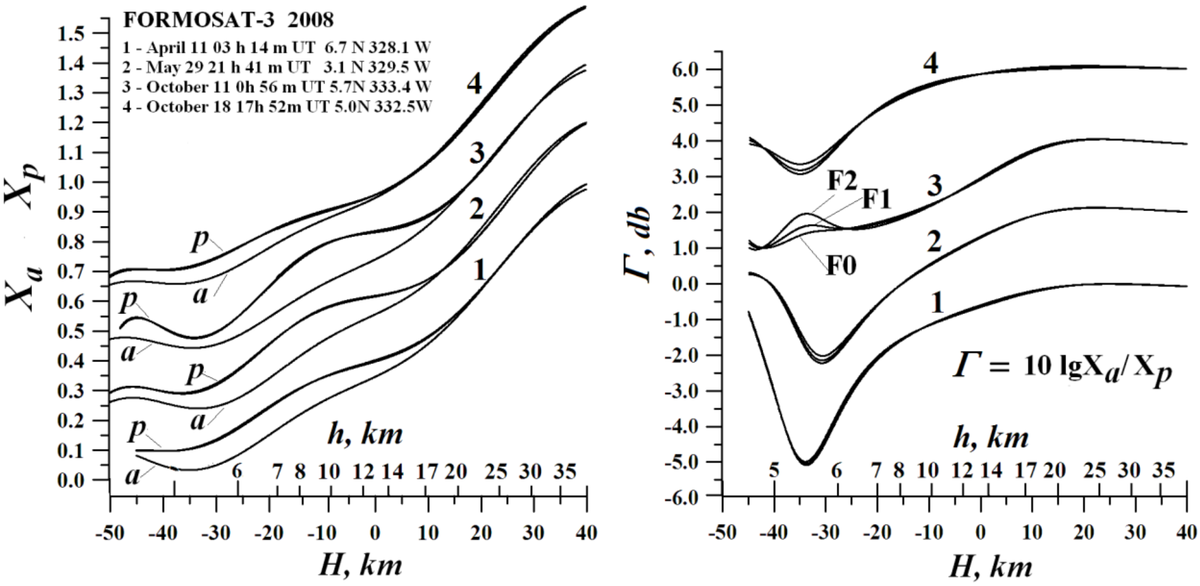
FORMOSAT-3 2008
1 - April 11 03 h 14 m UT 6.7 N 328.1 W
2 - May 29 21 h 41 m UT 3.1 N 329.5 W
3 - October 11 0h 56 m UT 5.7N 333.4 W
4 - October 18 17h 52m UT 5.0N 332.5W
Xa Xp
h, km
H, km
Γ, db
F2
F1
F0
Γ = 10 lgXa/Xp

Fig. 4

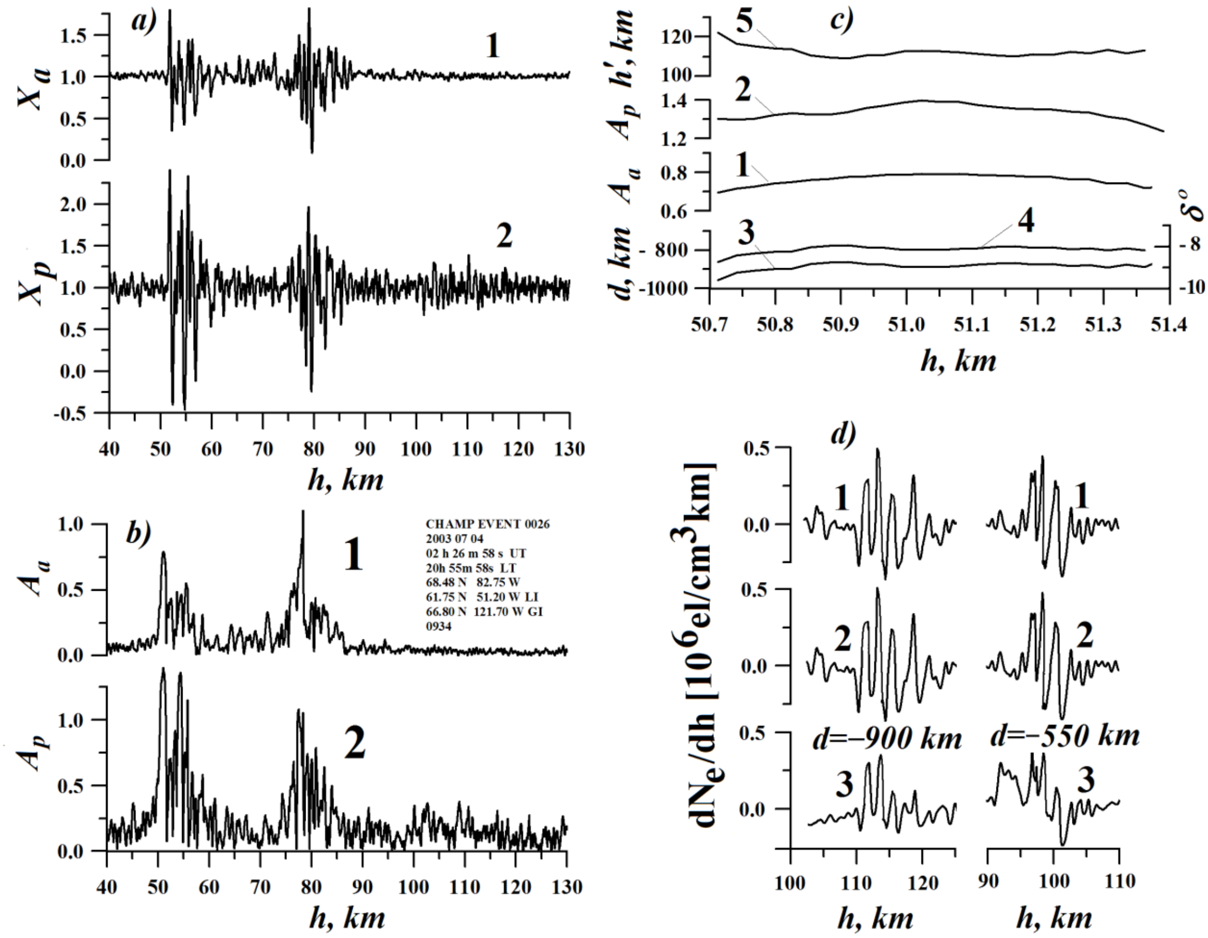
a)
b)
c)
d)
Xa
Xp
Aa
Ap
h, km
CHAMP EVENT 0026
2003 07 04
02 h 26 m 58 s UT
20h 55m 58s LT
68.48 N 82.75 W
61.75 N 51.20 W LI
66.80 N 121.70 W GI
0934
h', km
d, km
δ°
dNe/dh [10^6el/cm^3km]
d=–900 km
d=–550 km

Fig. 5

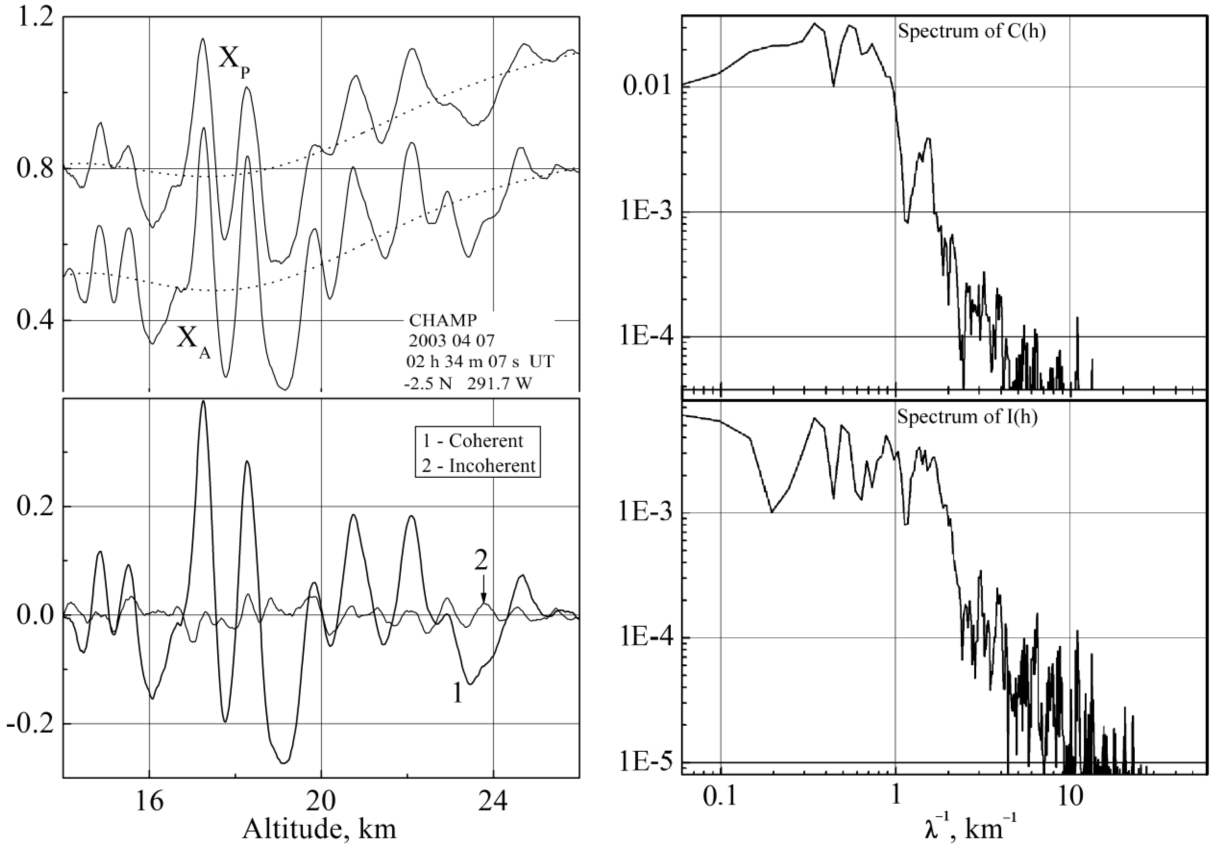

Fig. 6

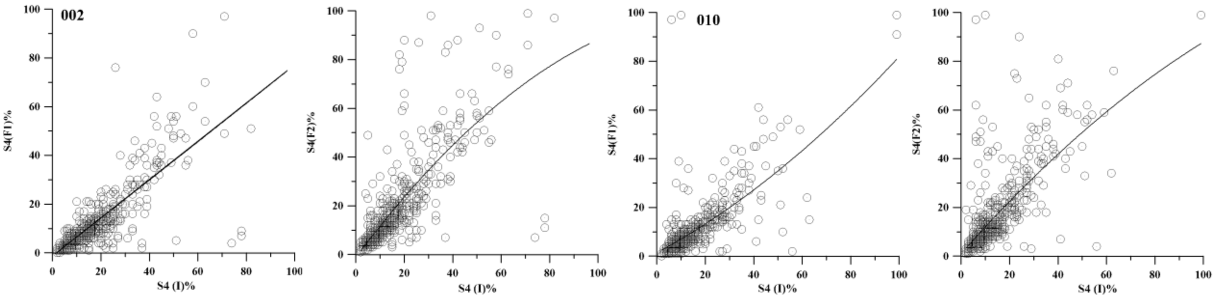

Fig. 7

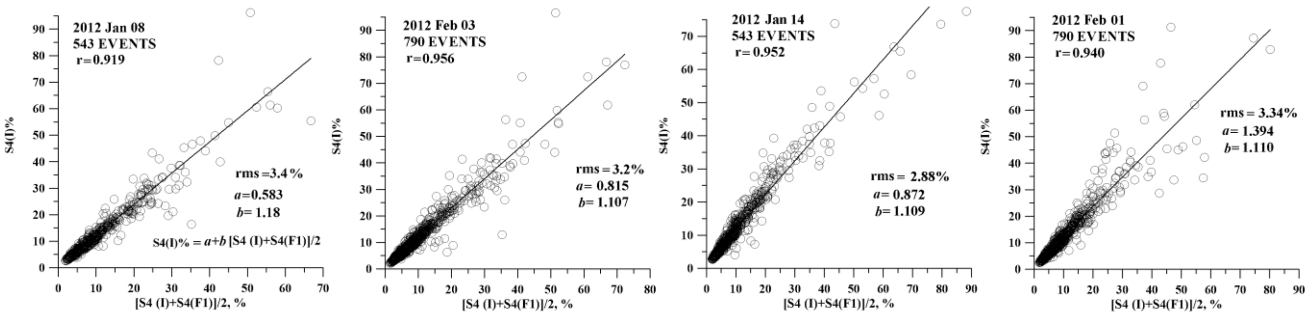

Fig. 8